Detection of oceanic electric fields based on the generalised likelihood ratio test (GLRT)

R. Donati and J.-P. Le Cadre

Abstract: Galvanic corrosion phenomena between the hull and the propeller of a ship induce static electric fields in sea water. These signatures can be observed on a vectorial electrical sensor and the authors investigate the design of a detection/localisation method based on the generalised maximum likelihood ratio test (GLRT). Incorporating a spatio-temporal analysis of the signals in the physical model, it is possible to partially estimate the trajectory of the target and to perform a detection decision. The resulting system consists in the calculation of the projection of the observation on a set of parameterised signatures and in selecting the projection that has the largest energy. An original method is proposed in order to determine the convenient partitioning of the set of projection bases. Due to the characteristics of the signals, classical results concerning performance analysis are not convenient and a specific framework is developed in order to analytically determine the behaviour of the system. A comparison with Monte Carlo simulations tends to prove the validity of the theory and the efficiency of the processing.

1 Introduction

Up to now, the only electromagnetic anomaly used to detect underwater targets has been the magnetostatic signatures due to their ferromagnetic nature [1–3]. However, other phenomena can generate electromagnetic fields, including galvanic corrosion between the hull and the propeller of a ship [4–6].

A circulation of electric currents, sometimes very powerful, in the sea water results from this chemical reaction and their static component induces a static electric field known as the UEP field (underwater electric potential). These signatures are measured with three-axis electrometers based either on current detection (the electric field being deduced from the measured current density via the microscopic Ohm's law) or on potential measurement (the electric field being then deduced by derivation).

The first stage (Section 2) of this paper is devoted to the development of an analytic model for the signatures radiated by a target. It is based on a dipolar representation of the ship and on the assumption of a three-layered medium made of air, sea water and the seabed. This structure induces multiple paths due to the interfaces between the air and the sea water and between the sea water and the seabed. Solving the Maxwell equations [7] for a source with a linear and uniform motion involves three unknown parameters: the ratio between the closest point of approach (CPA) and the velocity, the heading and the time of CPA. In this sense, the physical model includes target-motion analysis (TMA) aspects because the detection process fundamentally relies on a spatio-temporal analysis. Contrary to active array processing (e.g. radar and sonar), the contrast functional used here is built on TMA.

Then, the generalised likelihood ratio test (GLRT) [8] is applied to such signals (Section 3). It consists in estimating the kinematic parameters of the 'most probable' source by maximising the energy of projection of the observation on a set of synthetic normed signatures and then deciding if this target is present by comparing the maximum energy of projection to a threshold. The set of candidate signatures is obtained by defining a discretisation grid for the parameters covering all their possible values. The discretisation steps must be determined in order to minimise the size of the set while preserving the detection capabilities of the resulting system. For that purpose, an original scheme has been developed. It is based upon a distance measure very similar to the well known ambiguity concept.

The classical GLRT method is presented and embedded in the projector formalism in order to simplify the analytic determination of the performance (Section 4), both in terms of detection and localisation. Due to the particular characteristics of the observed signals (time-varying and time-limited), classical results for performance analysis [8, 9] are not convenient and some original calculations are required in order to predict, under the sole assumption of a strong enough signal-to-noise ratio (SNR), the behaviour of the system. More specifically, an analytic expression of the detection probability (based on the work of Villier [10]) was derived as well as a proof of the normality and the consistency of the trajectory estimator.

The results obtained by performing Monte Carlo simulations (Section 5) are then compared with theoretical predictions. The excellent agreement between them

IEE Proceedings online no. 20020491

DOI: 10.1049/ip-rsn:20020491

Paper first received 17th April 2000 and in final revised form 28th March 2002

R. Donati is with GESMA, Non Acoustic Detection Department, BP 42, 29240, Brest Naval, France
J.-P. Le Cadre is with IRISA/CNRS, Campus de Beaulieu, 35042, Rennes Cedex, France

validates the not only efficiency of the GLRT on the electrical signals but also the performance analysis.

An important aspect of this work is that, even if the GLRT is classicaly used in radar [11] or in various other domains, the spatial evolution of the target is then directly included in the used model of the signature. In other words, the GLRT directly performs the detection and the tracking of the target (under the assumption of a uniform rectilinear motion), as compared to the radar case where the use of the GLRT for target detection and target tracking implies the use of array processing methods. It is also worth noting that, in our problem, we have to process two time series (corresponding respectively to the X- and Y-axes of a single electrometer) observed by a single sensor, which makes the use of array processing methods impossible.

2 Electrical signals modelling

2.1 Electrical noise

Noise is assumed to be white and gaussian in the frequency band from 5×10^{-4} to 5×10^{-2} Hz which corresponds to the spectral bandwith of the signatures we wish to detect. This band is determined by considering the relative motion between the target and the sensor, as for magnetic signatures [1].

If the noise is not really white and gaussian, a whitening filter can be added and numerical bandpass filters, used in order to limit the observation to the frequency band of interest, should make the signal gaussian (it is a classical effect of numerical filtering operations produced by application of the large numbers law). In this paper, synthetic white gaussian noise has been used with a power spectral density equal to $100\,\mathrm{nV/m/(Hz)^{1/2}}$.

2.2 Electrical signatures

The model in use for the static field induced by corrosion effects is based upon a three-layer tabular modelling of the medium: air, sea water and seabed [6, 12]. As the context of this work is shallow waters (from 0 to 200 metres), the target is assumed to have a linear and uniform motion at a constant depth. It can be represented by an horizontal electric dipole.

The determination of the signatures radiated by such a target is relatively classic [5, 13]; it is based on the resolution of the well known Maxwell equations [5, 7] for a frequency equal to zero:

$$\begin{aligned} \boldsymbol{curl}(\boldsymbol{E}) + j\omega\mu_0\boldsymbol{H} &= \vec{\boldsymbol{0}}, \\ \boldsymbol{curl}(\boldsymbol{H}) - (j\omega\varepsilon + \sigma_1)\boldsymbol{E} &= Il \begin{vmatrix} \delta(\boldsymbol{r} - \boldsymbol{r}_s) \\ 0 \\ 0 \end{vmatrix} \end{aligned} \tag{1}$$

where $\boldsymbol{E}$ is the electric field, $\boldsymbol{H}$ is the magnetic field, ω is the angular frequency of the signal and σ, μ_0, ε are the constants of the medium ($j^2 = -1$). The Dirac function corresponds to the dipolar source of magnitude Il (I being the intensity of the corrosion currents and l the length of the line of current) oriented along the X-axis and localised at the position determined by the $\boldsymbol{r}_s(x_s, y_s, z_s)$ vector. In an homogeneous medium (i.e. an infinite sea), solving (1) leads to the following formulation of the three-dimensional electric field observed at the point $\boldsymbol{r}(x, y, z)$ [13]:

$$\boldsymbol{E} = \frac{Il}{4\pi\sigma_1} \begin{vmatrix} -\dfrac{1}{|\boldsymbol{r} - \boldsymbol{r}_s|^3} + 3\dfrac{(x - x_s)^2}{|\boldsymbol{r} - \boldsymbol{r}_s|^5} \\ 3\dfrac{(x - x_s)(y - y_s)}{|\boldsymbol{r} - \boldsymbol{r}_s|^5} \\ 3\dfrac{(x - x_s)(z - z_s)}{|\boldsymbol{r} - \boldsymbol{r}_s|^5} \end{vmatrix} \tag{2}$$

However, it is now necessary to take into account the different paths involved in the signal propagation, due to the reflections on the sea water/air and sea water/seabed interfaces when the water depth is equal to h. The incoming signal can:

- first reflect on the surface and then be affected by m double-reflections on both the seabed and the surface; so:

$$|\boldsymbol{r} - \boldsymbol{r}_{s1m}| = \sqrt{(x - x_s)^2 + (y - y_s)^2 + (z - 2mh + z_s)^2} \tag{3}$$

- first reflect on the seabed and then be affected by m double-reflections on both the seabed and the surface, yielding:

$$|\boldsymbol{r} - \boldsymbol{r}_{s2m}| = \sqrt{(x - x_s)^2 + (y - y_s)^2 + (z + 2mh + z_s)^2} \tag{4}$$

- first reflect on the surface and on the seabed and then be affected by m double-reflections on both the seabed and the surface; so:

$$|\boldsymbol{r} - \boldsymbol{r}_{s3m}| = \sqrt{(x - x_s)^2 + (y - y_s)^2 + (z + 2mh - z_s)^2} \tag{5}$$

- first reflect on the seabed and on the surface and then be affected by m double-reflections on both the seabed and the surface, yielding:

$$|\boldsymbol{r} - \boldsymbol{r}_{s4m}| = \sqrt{(x - x_s)^2 + (y - y_s)^2 + (z - 2mh - z_s)^2} \tag{6}$$

These different paths lead to many components for the signal collected at any point in the water and it is worth noting that the only difference between (3)–(6) is the vertical distance covered and the number of double-reflections (i.e. the term $z + \varepsilon mh + \varepsilon' z_s$ with $\varepsilon = \pm 1$ and $\varepsilon' = \pm 1$). For each path, (2) is valid when replacing $z - z_s$ by the total vertical distance covered by the signal and taking into account the fact that, for each reflection on the seabed, there is an attenuation equal to $A = (\sigma_1 - \sigma_2)/(\sigma_1 + \sigma_2)$, where σ_1 and σ_2 respectively correspond to the electrical conductivity of the sea water and the seabed.

Then, for a target trajectory which makes an angle denoted '*head*' with the X-axis of the sensor, the total field $\boldsymbol{E}$ observed at any point (x, y, z) in the water and expressed in cartesian coordinates linked to the sensor is as follows ($\boldsymbol{E}_{\text{target}}$ being the total field expressed in cartesian coordinates relative to the target):

$$\boldsymbol{E} = \begin{bmatrix} \cos(head) & -\sin(head) & 0 \\ \sin(head) & \cos(head) & 0 \\ 0 & 0 & 1 \end{bmatrix} \boldsymbol{E}_{\text{target}} \tag{7}$$

with:

$$\boldsymbol{E}_{\text{target}} = \frac{Il}{4\pi\sigma_1}\begin{vmatrix} -\dfrac{1}{|\boldsymbol{r}-\boldsymbol{r}_s|^3} + 3\dfrac{(x-x_s)^2}{|\boldsymbol{r}-\boldsymbol{r}_s|^5} + f_1(\boldsymbol{r}_{s10}, \boldsymbol{r}_{sim}) \\ 3\dfrac{(x-x_s)(y-y_s)}{|\boldsymbol{r}-\boldsymbol{r}_s|^5} + f_2(\boldsymbol{r}_{s10}, \boldsymbol{r}_{sim}) \\ 3\dfrac{(x-x_s)(z-z_s)}{|\boldsymbol{r}-\boldsymbol{r}_s|^5} + f_3(\boldsymbol{r}_{s10}, \boldsymbol{r}_{sim}) \end{vmatrix}$$

where

$$f_1(\boldsymbol{r}_{s10}, \boldsymbol{r}_{sim}) = -\frac{1}{|\boldsymbol{r}-\boldsymbol{r}_{s10}|^3} + 3\frac{(x-x_s)^2}{|\boldsymbol{r}-\boldsymbol{r}_{s10}|^5} + \sum_{i=1}^{4}\sum_{m=1}^{\infty} A^m\left(-\frac{1}{|\boldsymbol{r}-\boldsymbol{r}_{sim}|^3} + 3\frac{(x-x_s)^2}{|\boldsymbol{r}-\boldsymbol{r}_{sim}|^5}\right)$$

$$f_2(\boldsymbol{r}_{s10}, \boldsymbol{r}_{sim}) = 3\frac{(x-x_s)(y-y_s)}{|\boldsymbol{r}-\boldsymbol{r}_{s10}|^5} + \sum_{i=1}^{4}\sum_{m=1}^{\infty} A^m\left(3\frac{(x-x_s)(y-y_s)}{|\boldsymbol{r}-\boldsymbol{r}_{sim}|^5}\right)$$

$$f_3(\boldsymbol{r}_{s10}, \boldsymbol{r}_{sim}) = 3\frac{(x-x_s)(z+z_s)}{|\boldsymbol{r}-\boldsymbol{r}_{s10}|^5} + \sum_{i=1}^{4}\sum_{m=1}^{\infty} A^m\left(3\frac{(x-x_s)(z-z_{sim})}{|\boldsymbol{r}-\boldsymbol{r}_{sim}|^5}\right)$$

and:

$$\begin{aligned} p &= Il \\ x - x_s &= v(t_{CPA} - t) \\ y - y_s &= CPA \end{aligned} \tag{8}$$

In (8), CPA is the closest point of approach, that is to say the smallest distance between the sensor and the target. We can see that the three components of the electric field are real valued. In the expression, the infinite sum represents the different number of double-reflections (on the seabed and on the sea surface) corresponding to the various paths of the signal. Practically, due to the attenuation at each reflection on the seabed, it is sufficient to only consider the first 20 terms.

Hereafter, the vertical component will be neglected in this work because it is too weak to be observed. The sensor depth (z), the water depth (h) and the conductivities of the sea water and the seabed are known (in the area where the system is deployed) and some brief calculations and physical considerations show that the shape of the signatures is roughly independent of the target depth z_s (in shallow waters) as well as of both the CPA and the velocity v as long as the ratio CPA/v is constant. In our model, we can then fix the value of v and only deal with the ratio CPA/v.

Then, the observation only depends on four parameters:

- the ratio CPA/v,
- the time of CPA: t_{CPA},
- the angle between the heading of the target and the X-axis of the sensor, here denoted as '*head*',
- a magnitude coefficient k, that is a function of the electric moment of the source $p = Il$ and of the velocity of the target v.

An example of the electrical signatures is shown on Fig. 1 (with and without noise) for an electric moment equal to 50 Am (ampere metre). This represents the mean value of alternating electric moments measured on US merchant ships in Bostick *et al.* [14], assuming that the static electric moment is of the same order of magnitude (in fact, it is generally stronger).

On Fig. 1, the X-axis represents the time (in seconds) and the Y-axis the electric field in nanovolts per metre. The seabed conductivity is expressed in siemens per metre (S/m).

3 Detection with the generalised likelihood ratio test (GLRT)

3.1 Principle

The outputs of the two horizontal axes of the sensor, which are assumed to be temporally white, normal and correlated, are used simultaneously. Thus the total observation can be viewed as a sequence of N two-dimensional random vectors (t means 'transpose'):

$$\boldsymbol{z} = [\boldsymbol{z}_1, \boldsymbol{z}_2, \ldots, \boldsymbol{z}_N]^t = \left[\begin{pmatrix} x_1 \\ y_1 \end{pmatrix}, \begin{pmatrix} x_2 \\ y_2 \end{pmatrix}, \ldots, \begin{pmatrix} x_N \\ y_N \end{pmatrix}\right]^t \tag{9}$$

Due to the limited bandwidth of the signals we wish to detect, the sampling rate is typically 0.05 Hz and the number of samples N to consider can be taken to be equal to 100. Then, we have to deal with the two following hypotheses:

$$\begin{aligned} H_0 &: \boldsymbol{z}_i = \begin{pmatrix} x_i \\ y_i \end{pmatrix} = \begin{pmatrix} b_{xi} \\ b_{yi} \end{pmatrix} = \boldsymbol{b}_i, \\ H_1 &: \boldsymbol{z}_i = \begin{pmatrix} x_i \\ y_i \end{pmatrix} = \begin{pmatrix} b_{xi} \\ b_{yi} \end{pmatrix} + k\begin{pmatrix} E_x(\boldsymbol{\theta}, i) \\ E_y(\boldsymbol{\theta}, i) \end{pmatrix} \\ &= \boldsymbol{b}_i + k\boldsymbol{E}(\boldsymbol{\theta}, i) \end{aligned} \tag{10}$$

where k is the magnitude factor previously defined and $\boldsymbol{\theta}$ the vector of parameters containing CPA/v, the target heading and t_{CPA}. In (9) and (10), the signal $\boldsymbol{E}$ is given by (7) and (8) (for p and v being arbitrarily taken respectively equal to 1 Am and to 1 m/s, since the shape of $\boldsymbol{E}$ does not depend on v but only on the ratio CPA/v which is included in θ and b represents the noise described in subsection 2.1. The likelihood ratio stands as follows:

$$\Lambda(\boldsymbol{z}) = \frac{\exp\left[-\frac{1}{2}\sum_i (\boldsymbol{z}_i^t - k\boldsymbol{E}^t(\boldsymbol{\theta}, i))\boldsymbol{\Gamma}^{-1}(\boldsymbol{z}_i - k\boldsymbol{E}(\boldsymbol{\theta}, i))\right]}{\exp\left[-\frac{1}{2}\sum_i \boldsymbol{z}_i^t\boldsymbol{\Gamma}^{-1}\boldsymbol{z}_i\right]}$$

where:

$$\boldsymbol{\Gamma} = \boldsymbol{E}\{\boldsymbol{b}_i^t\boldsymbol{b}_i\} = \begin{bmatrix} \sigma_x^2 & \rho_{xy} \\ \rho_{xy} & \sigma_y^2 \end{bmatrix} \tag{11}$$

Now, keeping in mind that the matrix $\boldsymbol{\Gamma}$ is symmetric and positive definite, let $\boldsymbol{A}$ and $\boldsymbol{B}$ be two vectors having the same form as the observation $\boldsymbol{z}$, we can define a scalar product by:

$$\langle \boldsymbol{A}, \boldsymbol{B} \rangle = \sum_i (a_{i1}, a_{i2})\boldsymbol{\Gamma}^{-1}\begin{pmatrix} b_{i1} \\ b_{i2} \end{pmatrix} = \boldsymbol{A}\boldsymbol{\Sigma}^{-1}\boldsymbol{B}$$

with:

$$\boldsymbol{\Sigma} = \begin{bmatrix} \boldsymbol{\Gamma} & [0] & \cdots & [0] \\ [0] & \ddots & \ddots & \vdots \\ \vdots & \ddots & \ddots & [0] \\ [0] & \cdots & [0] & \boldsymbol{\Gamma} \end{bmatrix} \tag{12}$$

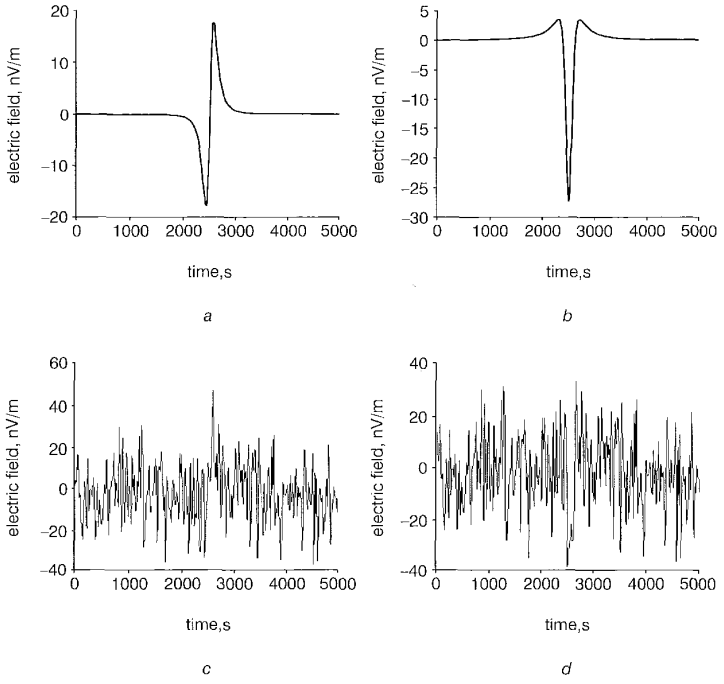

Fig. 1 *UEP signatures*
CPA = 600 m; *V* = 5 m/s; *head* = 90°; *p* = 50 Am; z_s = 100 m; *z* = 190 m
a *X*-axis without noise
b *Y*-axis without noise
c *X*-axis with noise
d *Y*-axis with noise

Then, the normalised signature vector $\boldsymbol{u}(\boldsymbol{\theta})$ is defined by normalised the vector $\boldsymbol{E}(\boldsymbol{\theta})$, i.e.:

$$\boldsymbol{s}(\boldsymbol{\theta}) = k\boldsymbol{E}(\boldsymbol{\theta}) = K\boldsymbol{u}(\boldsymbol{\theta})$$

with:

$$\boldsymbol{u}(\boldsymbol{\theta}) = \frac{\boldsymbol{E}(\boldsymbol{\theta})}{\sqrt{\langle \boldsymbol{E}(\boldsymbol{\theta}), \boldsymbol{E}(\boldsymbol{\theta})\rangle}} \tag{13}$$

where $\boldsymbol{s}(\boldsymbol{\theta})$ is the signature of the target received on the sensor. Then, by using this scalar product, the expression of the likelihood ratio becomes:

$$\Lambda(z) = \exp\left[-\frac{1}{2}(K^2 - 2K\langle z, \boldsymbol{u}(\boldsymbol{\theta})\rangle)\right] \tag{14}$$

so that:

$$\begin{aligned}\arg\max_{\boldsymbol{\theta},K}(\Lambda(z)) &= \arg\max_{\boldsymbol{\theta},K}(\log(\Lambda(z))) \\ &= \arg\max_{\boldsymbol{\theta},K}\left(-\frac{1}{2}(-2K\langle z, \boldsymbol{u}(\boldsymbol{\theta})\rangle + K^2)\right) \\ &= \arg\max_{\boldsymbol{\theta},K}\left(-\frac{1}{2}[(K - \langle z, \boldsymbol{u}(\boldsymbol{\theta})\rangle)^2 \right. \\ &\qquad \left. - \langle z, \boldsymbol{u}(\boldsymbol{\theta})\rangle^2]\right)\end{aligned} \tag{15}$$

and finally:

$$\hat{\boldsymbol{\theta}} = \arg\max_{\boldsymbol{\theta}}(\langle z, \boldsymbol{u}(\boldsymbol{\theta})\rangle^2) \quad \hat{K} = \langle z, \boldsymbol{u}(\hat{\boldsymbol{\theta}})\rangle \tag{16}$$

The parameter vector $\boldsymbol{\theta}$ is estimated by selecting the normed signal $\boldsymbol{u}(\boldsymbol{\theta})$ which maximises the energy of projection $\langle z, \boldsymbol{u}(\boldsymbol{\theta})\rangle^2$ (in the sense of the previously defined scalar product). K is then given by the norm of the projection.

So, a quantity of the form $|\boldsymbol{\Pi}_{\boldsymbol{\theta}}\boldsymbol{z}|^2$ is computed, where $\boldsymbol{\Pi}_{\boldsymbol{\theta}}$ is a projector parameterised by $\boldsymbol{\theta}$:

$$\boldsymbol{\Pi}_{\boldsymbol{\theta}} = \boldsymbol{u}(\boldsymbol{\theta})\boldsymbol{u}(\boldsymbol{\theta})^t\boldsymbol{\Sigma}^{-1} \tag{17}$$

The energy of projection, considered as a function of the parameter vector $\boldsymbol{\theta}$, is not concave. Moreover, the presence of local extrema means that gradient descent algorithms cannot be used. The only method available is to cursorily examine all the possible values of the parameters by using a discretisation grid. Then, by selecting the best one, we get a rough estimation of the parameters; the accuracy of which is limited by the stepsize of the grid. It is then possible to improve the estimation of the parameters by using a standard numerical optimisation code initialised by this rough estimation, i.e. in the vicinity of the global maximum.

Then, the decision that the estimated target is present is made conditionally to the test:

$$2\log(\Lambda(z)_{\boldsymbol{\theta}=\hat{\boldsymbol{\theta}}}) > \eta \Leftrightarrow \langle z, \boldsymbol{u}(\hat{\boldsymbol{\theta}})\rangle^2 > \eta \tag{18}$$

3.2 Discretisation of the signature parameters

First, even if the signature depends on four parameters, only three of them are involved in the expression of the basis of the signal space; K is only a magnitude factor.

So, the idea consists in discretising these three parameters with a sufficiently large stepsize in order to limit the computational load, but not too large in order to maintain the detection capabilities of the system. More precisely, we calculate the optimal stepsizes under the constraint that, whichever signal $\boldsymbol{s}(\boldsymbol{\theta})$ we might observe,

there exists in our system a normed signature $\boldsymbol{u}(\boldsymbol{\theta}+\Delta\boldsymbol{\theta})$ such that the energy of projection of the observation on this signature remains greater than or equal to 90% of the energy of projection of the observation upon $\boldsymbol{u}(\boldsymbol{\theta})$. Then, our algorithm consists in:

$$\min_{\Delta\boldsymbol{\theta}^-,\Delta\boldsymbol{\theta}^+} \prod_{i=1}^{3} \frac{\boldsymbol{\theta}_{i\max}-\boldsymbol{\theta}_{i\min}}{\Delta\boldsymbol{\theta}_i^+ + \Delta\boldsymbol{\theta}_i^-}$$

subject to:

$$\langle \boldsymbol{s}(\boldsymbol{\theta}), \boldsymbol{u}(\boldsymbol{\theta}+\Delta\boldsymbol{\theta})\rangle^2 > 0.9\langle \boldsymbol{s}(\boldsymbol{\theta}), \boldsymbol{u}(\boldsymbol{\theta})\rangle^2$$

with:

$$\boldsymbol{s}(\boldsymbol{\theta}) = \begin{pmatrix} \boldsymbol{s}_x(\boldsymbol{\theta}) \\ \boldsymbol{s}_y(\boldsymbol{\theta}) \end{pmatrix} = K \begin{pmatrix} \boldsymbol{u}_x(\boldsymbol{\theta}) \\ \boldsymbol{u}_y(\boldsymbol{\theta}) \end{pmatrix} \tag{19}$$

$$\Delta\boldsymbol{\theta} = (\Delta\boldsymbol{\theta}_1^+ \text{ or } \Delta\boldsymbol{\theta}_1^-, \Delta\boldsymbol{\theta}_2^+ \text{ or } \Delta\boldsymbol{\theta}_2^-, \Delta\boldsymbol{\theta}_3^+ \text{ or } \Delta\boldsymbol{\theta}_3^-)$$

$\boldsymbol{\theta}_{i\max}$ and $\boldsymbol{\theta}_{i\min}$ respectively correspond to the maximum and the minimum possible values of the parameter $\boldsymbol{\theta}_i$, $\Delta\boldsymbol{\theta}_i^+$ is the positive error by which $\boldsymbol{\theta}_i$ is affected and $\Delta\boldsymbol{\theta}_i^-$ the negative one. Then, for a given observed signature, we have to solve an optimisation problem with 2^3 constraints. In fact, we will show that only one of them must be verified.

More precisely, if $|\boldsymbol{\Pi}_{\boldsymbol{\theta}+\Delta\boldsymbol{\theta}}\boldsymbol{s}(\boldsymbol{\theta})|^2 = f(\boldsymbol{\theta}+\Delta\boldsymbol{\theta})$ is the energy of the projection of the signature, that is defined by the parameter $\boldsymbol{\theta}$ on the basis defined by the parameter $\boldsymbol{\theta}+\Delta\boldsymbol{\theta}$, and if $\Delta\boldsymbol{\theta}$ is assumed to be small, a second order expansion yields:

$$\begin{aligned} f(\boldsymbol{\theta}+\Delta\boldsymbol{\theta}) &= f(\boldsymbol{\theta}) + [\Delta\boldsymbol{\theta}]^t[\boldsymbol{grad}(f)(\boldsymbol{\theta})] \\ &\quad + \frac{1}{2}[\Delta\boldsymbol{\theta}]^t[\boldsymbol{hess}(f)(\boldsymbol{\theta})][\Delta\boldsymbol{\theta}] \\ &= f(\boldsymbol{\theta}) + \frac{1}{2}[\Delta\boldsymbol{\theta}]^t[\boldsymbol{hess}(f)(\boldsymbol{\theta})][\Delta\boldsymbol{\theta}] \end{aligned} \tag{20}$$

because the energy of the projection of the signature, that is defined by the parameter $\boldsymbol{\theta}$ on the basis defined by the parameter $\boldsymbol{\theta}$ is a maximum, thus implies that its gradient vector at this point is the null vector.

So, the relation $|\boldsymbol{\Pi}_{\boldsymbol{\theta}+\Delta\boldsymbol{\theta}}\boldsymbol{s}(\boldsymbol{\theta})|^2/|\boldsymbol{\Pi}_{\boldsymbol{\theta}}\boldsymbol{s}(\boldsymbol{\theta})|^2 = 0.9$ defines an ellipsoid centred around $\boldsymbol{\theta}$ and the optimisation problem consists in finding the largest solid rectangle inscribed in the ellipsoid. First, that implies that the solid rectangle is also centred around $\boldsymbol{\theta}$, and consequently that $\Delta\boldsymbol{\theta}_i^- = -\Delta\boldsymbol{\theta}_i^+$. It can be also inferred that the first vertex that reaches the ellipsoid when the solid rectangle increases is the one located in the quadrant containing the minor axis of the ellipsoid, that is to say the eigenvector associated with the largest eigenvalue of the hessian matrix.

Consequently, if this vertex is kept inside the ellipsoid, so will the others and verifying this sole constraint is equivalent to considering the 2^3 initial constraints. This is illustrated in Fig. 2 (for only two parameters).

This constraint must be simultaneously verified for all the signature types that we may observe, that is to say, for example, for these possible values of the parameters of the target:

- $CPA = 500$ or 2000 m
- velocity $= 2$ or 8 m/s
- course $= 0$ or 45°
- $t_{CPA} = 2500$ or 5000 s
- correlation coefficient between the noises on the X-axis and the Y-axis $= -0.8$ or 0 or 0.8

The quantification stepsizes obtained are:

- course: steps of 30° from 0 to 180°
- CPA/v: steps of 32 s from -2000 to 2000 s

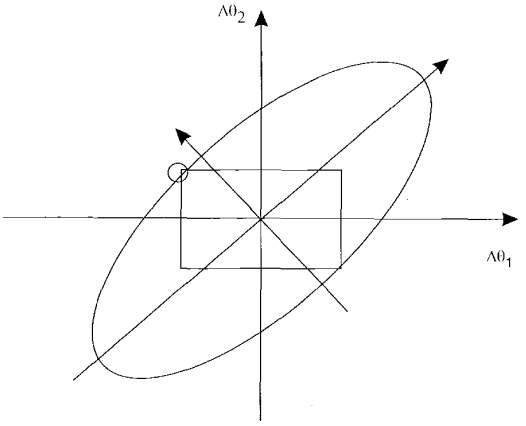

Fig. 2 *Geometric interpretation*

- time of CPA: steps of 20 s from 0 to 5000 s

That yields a set of about 100 000 bases of projection.

4 Schematic representation of the processing

The different tools useful for the detection of oceanic electric fields with the GLRT have been detailed in the preceding Sections and it is now possible to summarise the whole algorithm by the scheme represented on Fig. 3.

On this scheme, the signal model $\boldsymbol{E}$ corresponds to (8). It is worth keeping in mind that the maximisation is made by choosing the maximum output of the different branches, each branch corresponding to a particular value of the parameter vector of the signature model; the number of branches is consequently determined by the parameters' stepsizes evaluated in Section 3.2.

5 Performance analysis

5.1 False alarm probability

The definition of the false alarm probability is:

$$P_{\mathrm{FA}} = \mathrm{prob}[\max_{\boldsymbol{\theta}}\{\mathit{energy\_basis}(\boldsymbol{\theta})\} > \eta/H_0] \tag{21}$$

where $\mathit{energy\_basis}(\boldsymbol{\theta})$ is the energy of projection of the signal on the basis defined by the parameter $\boldsymbol{\theta}$.

The probability density function of each energy can first be calculated. As the noises are gaussian, it is straightforward to demonstrate that the quantity $\langle z, \boldsymbol{u}(\hat{\boldsymbol{\theta}})\rangle$ is a zero-mean gaussian random variable with a variance equal to:

$$\begin{aligned} \mathrm{var} &= \boldsymbol{E}\{\langle z, \boldsymbol{u}(\hat{\boldsymbol{\theta}})\rangle^2\} = \boldsymbol{E}\{(\boldsymbol{u}^t(\hat{\boldsymbol{\theta}})\boldsymbol{\Sigma}^{-1}z)^2\} \\ &= \boldsymbol{u}^t(\hat{\boldsymbol{\theta}})\boldsymbol{\Sigma}^{-1}[\boldsymbol{covar}(z)]\boldsymbol{\Sigma}^{-1}\boldsymbol{u}(\hat{\boldsymbol{\theta}}) = 1 \end{aligned} \tag{22}$$

Consequently, the probability density function of each energy of projection is a centred khi-2 with one degree of freedom.

However, the false alarm probability calculation suffers from many fundamental drawbacks. More precisely, if the energies of projection were all independent, the false alarm probability would be easily determined by:

$$\begin{aligned} P_{\mathrm{FA}} &= \mathrm{prob}[\max_{\boldsymbol{\theta}}\{\mathit{energy\_basis}(\boldsymbol{\theta})\} > \eta/H_0] \\ &= 1 - \mathrm{prob}[\mathit{all\_energies} < \eta/H_0] \\ &= 1 - \prod_{\boldsymbol{\theta}} \mathrm{prob}[\mathit{energy\_basis}(\boldsymbol{\theta}) < \eta/H_0] \end{aligned} \tag{23}$$

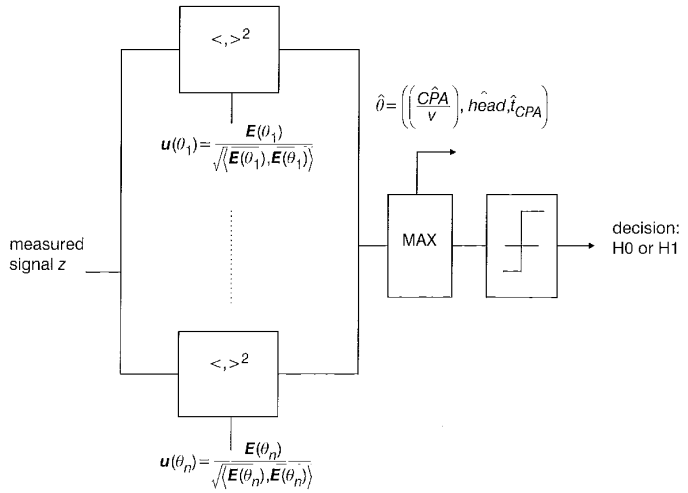

Fig. 3 *Scheme of the GLRT detector*

Unfortunately, they are not independent due to the fact that the bases of projection for different values of the parameters are not orthogonal. In order to calculate the P_{FA}, it would be necessary to determine all the correlations between the various energies, that is to say

$$\binom{2}{n}$$

correlations ($=n(n-1)/2$). As $n=100\,000$, this is clearly unfeasible.

It is worth mentioning another approach for calculating the P_{FA} which heavily relies upon differential geometry [10]. But the major drawback of this method is that it is only valid for weak values of the P_{FA} (<0.1). So, it is not convenient for the calculation of a complete ROC (receiver operating characteristics) curve.

A third approach that could have enabled us to calculate the P_{FA} is the Wilks's theorem [9] which demonstrates that, if the random vectors z_i are independent identically distributed under both the H_0 and H_1 hypotheses, then under H_0:

$$2\log(\Lambda(z)_{\boldsymbol{\theta}=\hat{\boldsymbol{\theta}}}) \rightarrow \chi^2_r \tag{24}$$

where r is the number of parameters. However, in our problem, the samples are not identically distributed under H_1 because the mean value of each sample is then equal to the signature of the target which is a time-varying signal.

The conclusion is that for such a system, the analytic calculation of the false alarm probability seems impossible and the only practical solution is to perform Monte Carlo simulations. This point has already been identified in Friedlander and Porat [15, 16]; in order to avoid it, a suboptimal version of the GLRT is proposed, consisting in splitting the observed data into two sets, the first one being used to give an estimate of the signal parameters under H_0 and the second one to make the detection. The main drawbacks are that this method is limited to the case of white noises and that it results in a decrease of the detection probability.

Fortunately, the determination of the P_{FA} by simulations is not a real problem for us because the P_{FA} only depends on the set of bases of projection (which is fixed) and on the characteristics of the noises. So, the false alarm probability can be determined by simulations during a learning stage of the system and then be considered known when the detector is operational.

5.2 Detection probability

Surprisingly, the determination of the detection probability is less problematic. Our demonstration is detailed in the Appendix but we will now present the main results.

Our work is based on the assumption that, as the observed signal is embedded in noise, the energy of projection will not be a maximum for the real value of the parameters but rather for a value $\hat{\boldsymbol{\theta}}$ close to the real value. Then, we can expand the energy of projection up to the second order:

$$|\boldsymbol{\Pi}_{\hat{\boldsymbol{\theta}}}\boldsymbol{z}|^2 = f(\hat{\boldsymbol{\theta}}) = f(\boldsymbol{\theta}) + [\hat{\boldsymbol{\theta}}-\boldsymbol{\theta}]^t[\boldsymbol{grad}(f)(\boldsymbol{\theta})] + \frac{1}{2}[\hat{\boldsymbol{\theta}}-\boldsymbol{\theta}]^t[\boldsymbol{hess}(f)(\boldsymbol{\theta})][\hat{\boldsymbol{\theta}}-\boldsymbol{\theta}] \tag{25}$$

and we then find that its maximum value is given by:

$$\sup_{\hat{\boldsymbol{\theta}}} f(\hat{\boldsymbol{\theta}}) = f(\boldsymbol{\theta}) - \frac{1}{2}[\boldsymbol{grad}(f)(\boldsymbol{\theta})]^t[\boldsymbol{hess}(f)(\boldsymbol{\theta})]^{-1} \times [\boldsymbol{grad}(f)(\boldsymbol{\theta})] \tag{26}$$

Now, calculations presented in the Appendix give that:

$$[\boldsymbol{hess}(f)(\boldsymbol{\theta})] \cong \left[\boldsymbol{s}^t\boldsymbol{\Sigma}^{-1}\frac{\partial^2\boldsymbol{\Pi}_{\boldsymbol{\theta}}}{\partial\theta_i\partial\theta_j}\boldsymbol{s}\right]_{\substack{i=1,\ldots,p\\ j=1,\ldots,p}} = -2\left[K^2\frac{\partial\boldsymbol{u}^t}{\partial\theta_i}\boldsymbol{\Sigma}^{-1}\frac{\partial\boldsymbol{u}}{\partial\theta_j}\right]_{\substack{i=1,\ldots,p\\ j=1,\ldots,p}} \tag{27}$$

$$[\boldsymbol{grad}(f)(\boldsymbol{\theta})] \cong \begin{bmatrix} 2K\dfrac{\partial\boldsymbol{u}^t}{\partial\theta_1}\boldsymbol{\Sigma}^{-1}\boldsymbol{b} \\ \vdots \\ 2K\dfrac{\partial\boldsymbol{u}^t}{\partial\theta_p}\boldsymbol{\Sigma}^{-1}\boldsymbol{b} \end{bmatrix} \rightarrow N\left(\begin{bmatrix}0\\ \vdots \\ 0\end{bmatrix}, \left[4K^2\frac{\partial\boldsymbol{u}^t}{\partial\theta_i}\boldsymbol{\Sigma}^{-1}\frac{\partial\boldsymbol{u}}{\partial\theta_j}\right]_{\substack{i=1,\ldots,p\\ j=1,\ldots,p}}\right) \tag{28}$$

Then, we show that:

$$-\frac{1}{2}[\boldsymbol{grad}(f)(\boldsymbol{\theta})]^t[\boldsymbol{hess}(f)(\boldsymbol{\theta})]^{-1}[\boldsymbol{grad}(f)(\boldsymbol{\theta})] \rightarrow \chi^2_p \tag{29}$$

with $p=3$. Now, by demonstrating the fact that this random variable is independent of $f(\boldsymbol{\theta})$ which is the square of a gaussian random variable equal to:

$$\langle \boldsymbol{z}, \boldsymbol{u} \rangle = K + \boldsymbol{u}^t \boldsymbol{\Sigma}^{-1} \boldsymbol{b} \tag{30}$$

we arrive at the conclusion that the probability density function of the maximum of the projection energies is a non-central khi-2 with $1+p=4$ degrees of freedom:

$$\sup_{\hat{\boldsymbol{\theta}}} f(\hat{\boldsymbol{\theta}}) = \sup_{\hat{\boldsymbol{\theta}}} |\boldsymbol{\Pi}_{\hat{\boldsymbol{\theta}}} \boldsymbol{z}|^2 = 2 \log(\Lambda(\boldsymbol{z})_{\boldsymbol{\theta}=\hat{\boldsymbol{\theta}}}) \rightarrow \chi^2_4(K^2) \tag{31}$$

This result is the same as the ones given by Kendall and Stuart [17] and also Zhu and Haykin [11] but its validity is no longer limited to the case of independent identically distributed samples and we have established that this assumption is not required as long as the SNR remains strong enough. This result enables us to compute the operational characteristics of the detector. This point will be developed in Section 6.

5.3 Cramer–Rao lower bounds (CRLB)

The calculation of the Cramer–Rao Lower Bounds (CRLB) of the estimators requires the determination of the Fisher information matrix $\boldsymbol{FIM}_{\boldsymbol{\theta}}$:

$$E\{(\hat{\boldsymbol{\theta}} - \boldsymbol{\theta})^T (\hat{\boldsymbol{\theta}} - \boldsymbol{\theta})\} \geq \boldsymbol{FIM}_{\boldsymbol{\theta}}^{-1}$$

with:

$$[\boldsymbol{FIM}_{\boldsymbol{\theta}}]_{ij} = \boldsymbol{E}\left\{ \left[\frac{\partial}{\partial \theta_i} \log p_{\boldsymbol{\theta}}(\boldsymbol{z}) \right] \left[\frac{\partial}{\partial \theta_j} \log p_{\boldsymbol{\theta}}(\boldsymbol{z}) \right] \right\} \tag{32}$$

In (32), $p_{\boldsymbol{\theta}}(\boldsymbol{z})$ is the probability density function of the observation $\boldsymbol{z}$ conditionally to the parameter $\boldsymbol{\theta}$. The sign 'greater than or equal to' means that the difference between the two matrices is non-negative definite.
Under the assumption of a normal observation:

$$p_{\boldsymbol{\theta}}(\boldsymbol{z}) = \boldsymbol{A} \exp\left[-\frac{1}{2} \langle (\boldsymbol{z} - \boldsymbol{K}\boldsymbol{u}(\boldsymbol{\theta})), (\boldsymbol{z} - \boldsymbol{K}\boldsymbol{u}(\boldsymbol{\theta})) \rangle \right] \tag{33}$$

so that:

$$\frac{\partial}{\partial \theta_i} \log p_{\boldsymbol{\theta}}(\boldsymbol{z}) = \left\langle (\boldsymbol{z} - \boldsymbol{K}\boldsymbol{u}(\boldsymbol{\theta})), \boldsymbol{K} \frac{\partial \boldsymbol{u}(\boldsymbol{\theta})}{\partial \theta_i} \right\rangle \tag{34}$$

and finally:

$$\begin{aligned} [\boldsymbol{FIM}_{\boldsymbol{\theta}}]_{ij} &= \left[\boldsymbol{K}^2 \left\langle \frac{\partial \boldsymbol{u}(\boldsymbol{\theta})}{\partial \theta_i}, \frac{\partial \boldsymbol{u}(\boldsymbol{\theta})}{\partial \theta_j} \right\rangle \right]_{ij} \\ &= \left[\boldsymbol{K}^2 \frac{\partial \boldsymbol{u}(\boldsymbol{\theta})^t}{\partial \theta_i} \boldsymbol{\Sigma}^{-1} \frac{\partial \boldsymbol{u}(\boldsymbol{\theta})}{\partial \theta_j} \right]_{ij} \end{aligned} \tag{35}$$

target is far enough away, they become identically equal to zero, regardless of the value of the parameters of the target. So, they do not apply to our problem.

Nevertheless, if we assume that the SNR is strong enough, it is possible to establish the normality and the consistency of our estimator by using the results of our calculation of the detection probability. In fact:

$$[\hat{\boldsymbol{\theta}} - \boldsymbol{\theta}] = -[\boldsymbol{hess}(f)(\boldsymbol{\theta})]^{-1} [\boldsymbol{grad}(f)(\boldsymbol{\theta})] \tag{36}$$

and under the hypothesis of a strong enough SNR, we have:

$$\begin{aligned} [\boldsymbol{grad}(f)(\boldsymbol{\theta})] &\cong \begin{bmatrix} 2K \dfrac{\partial \boldsymbol{u}^t}{\partial \theta_1} \boldsymbol{\Sigma}^{-1} \boldsymbol{b} \\ \vdots \\ 2K \dfrac{\partial \boldsymbol{u}^t}{\partial \theta_p} \boldsymbol{\Sigma}^{-1} \boldsymbol{b} \end{bmatrix} \\ &\rightarrow N\left(\begin{bmatrix} 0 \\ \vdots \\ 0 \end{bmatrix}, \left[4K^2 \frac{\partial \boldsymbol{u}^t}{\partial \theta_i} \boldsymbol{\Sigma}^{-1} \frac{\partial \boldsymbol{u}}{\partial \theta_j} \right]_{\substack{i=1,\ldots,p \\ j=1,\ldots,p}} \right) \end{aligned} \tag{37}$$

$$\begin{aligned} [\boldsymbol{hess}(f)(\boldsymbol{\theta})] &\cong \left[\boldsymbol{s}^t \boldsymbol{\Sigma}^{-1} \frac{\partial^2 \boldsymbol{\Pi}_{\boldsymbol{\theta}}}{\partial \theta_i \partial \theta_j} \boldsymbol{s} \right]_{\substack{i=1,\ldots,p \\ j=1,\ldots,p}} \\ &= -2 \left[K^2 \frac{\partial \boldsymbol{u}^t}{\partial \theta_i} \boldsymbol{\Sigma}^{-1} \frac{\partial \boldsymbol{u}}{\partial \theta_j} \right]_{\substack{i=1,\ldots,p \\ j=1,\ldots,p}} \end{aligned} \tag{38}$$

So, it is straightforward to deduce that:

$$\begin{aligned} [\hat{\boldsymbol{\theta}} - \boldsymbol{\theta}] &\rightarrow N\left(\begin{bmatrix} 0 \\ \vdots \\ 0 \end{bmatrix}, \left[K^2 \frac{\partial \boldsymbol{u}^t}{\partial \theta_i} \boldsymbol{\Sigma}^{-1} \frac{\partial \boldsymbol{u}}{\partial \theta_j} \right]^{-1}_{\substack{i=1,\ldots,p \\ j=1,\ldots,p}} \right) \\ &= N\left(\begin{bmatrix} 0 \\ \vdots \\ 0 \end{bmatrix}, [\boldsymbol{FIM}_{\boldsymbol{\theta}}]^{-1}_{\substack{i=1,\ldots,p \\ j=1,\ldots,p}} \right) \end{aligned} \tag{39}$$

So, we see that the MLE estimator has a rather 'classical' behaviour despite non-stationarity and time-limited signals.

6 Simulations

In Fig. 4, the results of Monte Carlo simulations (for the signals represented in Fig. 1) are presented and compared with their theoretical counterpart. The left-hand sides of Figs. 4*a*, *b* and *c* represent the histograms of the estimators for a target whose kinematic parameters are given in the figure caption. Their theoretical probability density functions (pdf) (which are normal functions centred on the true values of the parameters and with variances equal to the CRLB) are also plotted in the right-hand sides of these Figures. In Fig. 4*d*, we present the ROC curve obtained by simulation, for a far away target in order to make the curve easier to read, and compare it with the 'theoretical/ simulation' curve for which the detection probability was analytically calculated and the false alarm probability was determined by simulation.

Good agreement between the theoretical results and the simulations is obtained, both for detection and estimation, with a very low SNR (see Fig. 1). The estimators are almost optimal, they reach the Cramer–Rao lower bounds,

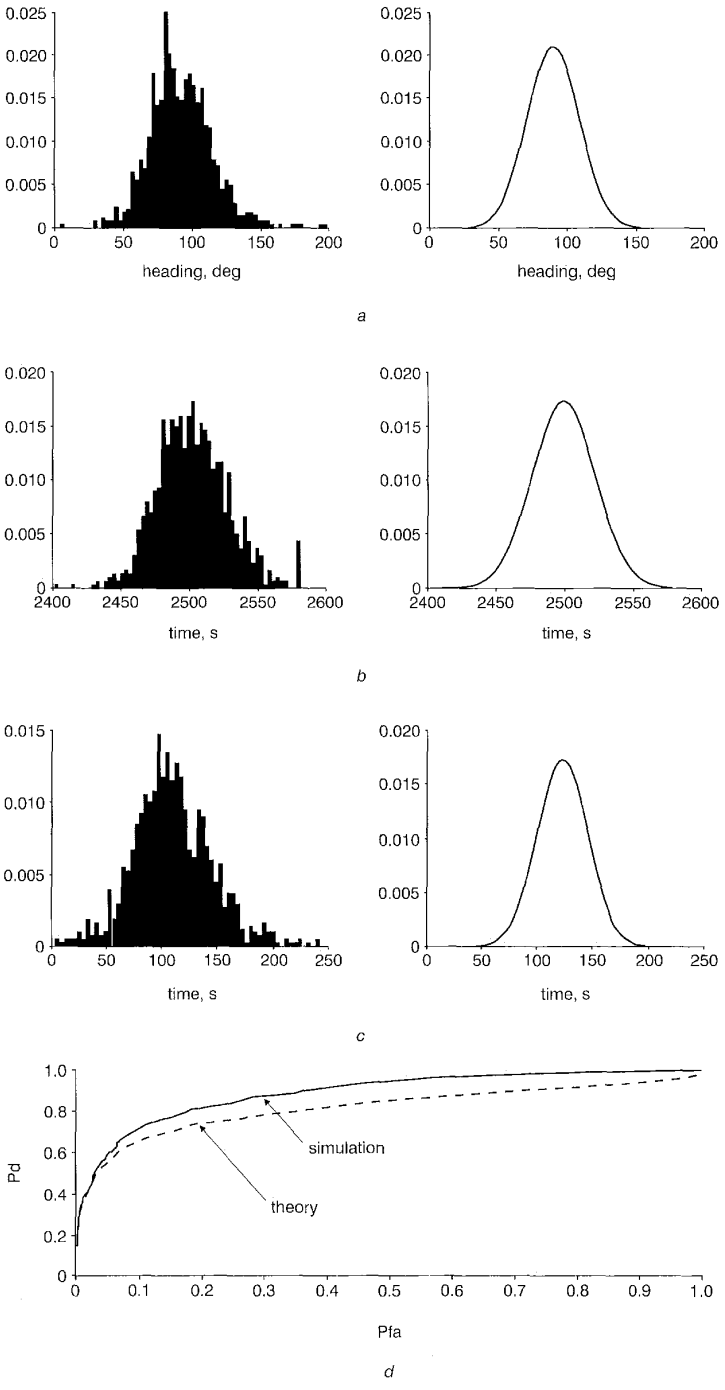

Fig. 4 *Performance of the system*

$CPA = 800$ m; $V = 5$ m/s; $head = 90°$; $p = 50$ Am; $z_s = 100$ m; $z = 190$ m; $h = 200$ m; and $\sigma_2 = 0.01$ s/m

a Histogram and theoretical pdf of the estimator of the heading

b Histogram and theoretical pdf of the estimator of the time of *CPA*

c Histogram and theoretical pdf of the estimator of *CPA*/*v*

d ROC curve

they are gaussian and consistent, the *CPA*/*v* estimator excepted, which is affected by a small bias.

This bias can be justified by the fact that the dependency of our physical model upon the single ratio *CPA*/*v* (and not upon both *CPA* and *v*) implies greater horizontal distances compared with the vertical distances. In our simulations, with a *CPA* distance equal to 600 m and a water depth equal to 200 m, this assumption is not completely realistic and the shape of the signature depends on both *CPA* and *v*.

The theoretical detection probability also presents a good agreement with the simulation results; the error is always less than 10% and even less for small values of the false alarm probability (which will be the case for an operational system).

7 Conclusions

This work has shown the potentialities of a detection/localisation system based on the application of the GLRT on the observation collected on a vectorial UEP sensor. Spatio-temporal processing has been directly incorporated in the physical model of the target signatures and a realistic performance analysis has been developed. Due to particular assumptions, classical results for performance analysis do not hold; this leads us to consider a specific framework which is general and applicable to many other problems. Original results have been established. They enable us to accurately predict the behaviour of our system both for detection and estimation. These approximations are valid under mild hypotheses.

Good detection and estimation capabilities for our system have been demonstrated, both in theory and simulations. The theory has been presented in a unified formalism and gave results which might be instrumental in the development of a multisensor system.

8 References

1 CARITU, Y.: 'Système de détection/localisation de mobile ferromagnétique par un réseau de magnétomètres haute sensibilité'. PhD thesis, Institut National Polytechnique de Grenoble, 1996
2 CHICHEREAU, C.: 'Traitement de réseaux magnétiques – réduction des phénomènes perturbateurs pour la détection-localisation'. PhD thesis, Institut National Polytechnique de Grenoble, 1996
3 DASSOT, G.: 'Réseaux multicapteurs pour la surveillance de zones océaniques'. PhD thesis, Institut National Polytechnique de Grenoble, 1997
4 COLLEE, R.: 'Corrosion marine' (Editions CEBEDOC, 1975)
5 VRBANCICH, J., ANDREAUS, M., DONOHOO, A., and TURNBULL, S.J.: 'Corrosion induced electromagnetic and electrostatic fields'. Proceedings of Marelec 1997, London, June 1997
6 ASRAF, D., NEDGARD, I., and KRYLSTEDT, P.: 'On static electric source for underwater target tracking in shallow water environments'. Proceedings of HYAK 1997, London, September 1997
7 FOURNET, G.: 'Electromagnétisme à partir des équations locales' (Masson, 1980, 2nd edn.)
8 POOR, H.V.: 'An introduction to signal detection and estimation' (Springer-Verlag, 1994, 2nd edn.)
9 FERGUSON, T.S.: 'A course in large sample theory' (Chapman & Hall, 1996, 1st edn.)
10 VILLIER, E.: 'Contribution aux méthodes à sous-espaces en traitement du signal'. PhD thesis, Université de Rennes I, 1995
11 ZHU, Z., and HAYKIN, S.: 'Radar detection using array processing' (Springer-Verlag, 1993)
12 BRUXELLE, J.Y.: 'Champs electriques statiques en detection sous-marine'. Rapport GESMA No. 4079 du 16 mars 1995
13 DONATI, R.: 'Détection de signaux électriques océaniques – Application à la surveillance de zones'. PhD thesis, Université de Rennes I, 2000
14 BOSTICK, F.X., SMITH, H.W., and BOEH, J.E.: 'The detection of ULF, ELF emission of moving ships'. Final Report AD A037 830, Electrical Engineering Research Laboratory, University of Texas, Austin, TX, 1977
15 FRIEDLANDER, B., and PORAT, B.: 'Performance analysis of transient detectors based on a class of linear data transforms', *IEEE Trans. Inf. Theory*, March 1992, **37**, (5), pp. 665–673
16 FRIEDLANDER, B., and PORAT, B.: 'On the generalized maximum likelihood ratio test for a class of nonlinear detection problems', *IEEE Trans. Signal Process.*, 1993, **41**, (11), pp. 3186–3190
17 KENDALL, M., and STUART, A.: 'The advanced theory of statistics, Vol. 2' (Macmillan, New York, 1974)
18 KAY, S.M.: 'Asymptotically optimal detection in incompletely characterized non-Gaussian noise', *IEEE Trans. Acoust. Speech Signal Process.*, 1989, **37**, (5), pp. 627–633

9 Appendix

Our calculation of the detection probability follows the general guidelines of Villier [10]. Our calculation slightly differs from that of Villier [10] and constitutes a generalisation to the case of a multi-dimensional vector of parameters.

Our work is based on the assumption that, as the observed signal is embedded in noise, the energy of projection will not be a maximum for the real value of the parameters but rather for a value $\hat{\boldsymbol{\theta}}$ close to the real value. Then, we can expand the energy of projection up to the second order:

$$\left|\boldsymbol{\Pi}_{\hat{\boldsymbol{\theta}}}\boldsymbol{z}\right|^2 = f(\hat{\boldsymbol{\theta}}) = f(\boldsymbol{\theta}) + [\hat{\boldsymbol{\theta}} - \boldsymbol{\theta}]^t[\boldsymbol{grad}(f)(\boldsymbol{\theta})] + \frac{1}{2}[\hat{\boldsymbol{\theta}} - \boldsymbol{\theta}]^t[\boldsymbol{hess}(f)(\boldsymbol{\theta})][\hat{\boldsymbol{\theta}} - \boldsymbol{\theta}] \quad (40)$$

Differentiating (40), it appears that the function $f(\hat{\boldsymbol{\theta}})$ is a maximum for:

$$[\hat{\boldsymbol{\theta}} - \boldsymbol{\theta}] = -[\boldsymbol{hess}(f)(\boldsymbol{\theta})]^{-1}[\boldsymbol{grad}(f)(\boldsymbol{\theta})] \quad (41)$$

Substituting the value given by (41) in (40), we have:

$$\sup_{\hat{\boldsymbol{\theta}}} f(\hat{\boldsymbol{\theta}}) = f(\boldsymbol{\theta}) - \frac{1}{2}[\boldsymbol{grad}(f)(\boldsymbol{\theta})]^t[\boldsymbol{hess}(f)(\boldsymbol{\theta})]^{-1} \times [\boldsymbol{grad}(f)(\boldsymbol{\theta})] \quad (42)$$

Using the general properties of projectors, and more precisely the fact that $\langle \boldsymbol{\Pi}_{\boldsymbol{\theta}}\boldsymbol{z}, \boldsymbol{\Pi}_{\boldsymbol{\theta}}\boldsymbol{z}\rangle = \langle \boldsymbol{z}, \boldsymbol{\Pi}_{\boldsymbol{\theta}}\boldsymbol{z}\rangle$, we can write that:

$$[\boldsymbol{grad}(f)(\boldsymbol{\theta})] = \left[\boldsymbol{grad}\left(\left|\boldsymbol{\Pi}_{\boldsymbol{\theta}}\boldsymbol{z}\right|^2\right)\right] = \left[\boldsymbol{grad}\left(\langle \boldsymbol{\Pi}_{\boldsymbol{\theta}}\boldsymbol{z}, \boldsymbol{\Pi}_{\boldsymbol{\theta}}\boldsymbol{z}\rangle\right)\right] = \left[\boldsymbol{grad}\left(\langle \boldsymbol{z}, \boldsymbol{\Pi}_{\boldsymbol{\theta}}\boldsymbol{z}\rangle\right)\right] \quad (43)$$

with:

$$\left[\boldsymbol{grad}\left(\langle \boldsymbol{z}, \boldsymbol{\Pi}_{\boldsymbol{\theta}}\boldsymbol{z}\rangle\right)\right] = \left[\boldsymbol{grad}\left(\boldsymbol{z}^t\boldsymbol{\Sigma}^{-1}\boldsymbol{\Pi}_{\boldsymbol{\theta}}\boldsymbol{z}\right)\right] \quad (44)$$

So, replacing $\boldsymbol{z}$ by $\boldsymbol{s}+\boldsymbol{b}$ where $\boldsymbol{s} = K\boldsymbol{u}(\boldsymbol{\theta})$ is the observed signature and $\boldsymbol{b}$ the noise in which it is embedded, we have:

$$[\boldsymbol{grad}(f)(\boldsymbol{\theta})] = \left[\boldsymbol{s}^t\boldsymbol{\Sigma}^{-1}\frac{\partial \boldsymbol{\Pi}_{\boldsymbol{\theta}}}{\partial\theta_i}\boldsymbol{s}\right]_{i=1,\ldots,p} + 2\left[\boldsymbol{b}^t\boldsymbol{\Sigma}^{-1}\frac{\partial \boldsymbol{\Pi}_{\boldsymbol{\theta}}}{\partial\theta_i}\boldsymbol{s}\right]_{i=1,\ldots,p} + \left[\boldsymbol{b}^t\boldsymbol{\Sigma}^{-1}\frac{\partial \boldsymbol{\Pi}_{\boldsymbol{\theta}}}{\partial\theta_i}\boldsymbol{b}\right]_{i=1,\ldots,p} \quad (45)$$

We can similarly calculate the expression of the hessian matrix:

$$[\boldsymbol{hess}(f)(\boldsymbol{\theta})] = \left[\boldsymbol{s}^t\boldsymbol{\Sigma}^{-1}\frac{\partial^2 \boldsymbol{\Pi}_{\boldsymbol{\theta}}}{\partial\theta_i\partial\theta_j}\boldsymbol{s}\right]_{\substack{i=1,\ldots,p\\ j=1,\ldots,p}} + 2\left[\boldsymbol{s}^t\boldsymbol{\Sigma}^{-1}\frac{\partial^2 \boldsymbol{\Pi}_{\boldsymbol{\theta}}}{\partial\theta_i\partial\theta_j}\boldsymbol{b}\right]_{\substack{i=1,\ldots,p\\ j=1,\ldots,p}} + \left[\boldsymbol{b}^t\boldsymbol{\Sigma}^{-1}\frac{\partial^2 \boldsymbol{\Pi}_{\boldsymbol{\theta}}}{\partial\theta_i\partial\theta_j}\boldsymbol{b}\right]_{\substack{i=1,\ldots,p\\ j=1,\ldots,p}} \quad (46)$$

Now, using the equality $\|\boldsymbol{u}\| = 1$, we obtain:

$$\left\langle \boldsymbol{u}, \frac{\partial \boldsymbol{u}}{\partial\theta_i}\right\rangle = \boldsymbol{u}^t\boldsymbol{\Sigma}^{-1}\frac{\partial \boldsymbol{u}}{\partial\theta_i} = 0 \quad (47)$$

and again differentiating (47):

$$\frac{\partial \boldsymbol{u}^t}{\partial\theta_i}\boldsymbol{\Sigma}^{-1}\frac{\partial \boldsymbol{u}}{\partial\theta_j} + \boldsymbol{u}^t\boldsymbol{\Sigma}^{-1}\frac{\partial^2 \boldsymbol{u}}{\partial\theta_i\partial\theta_j} = 0 \quad (48)$$

Differentiating the expression of the projector (17) also gives:

$$\frac{\partial \boldsymbol{\Pi}_{\boldsymbol{\theta}}}{\partial\theta_i} = \frac{\partial \boldsymbol{u}}{\partial\theta_i}\boldsymbol{u}^t\boldsymbol{\Sigma}^{-1} + \boldsymbol{u}\frac{\partial \boldsymbol{u}^t}{\partial\theta_i}\boldsymbol{\Sigma}^{-1} \quad (49)$$

from which it can be inferred that:

$$\boldsymbol{u}^t\boldsymbol{\Sigma}^{-1}\frac{\partial \boldsymbol{\Pi}_{\boldsymbol{\theta}}}{\partial \theta_i}=\frac{\partial \boldsymbol{u}^t}{\partial \theta_i}\boldsymbol{\Sigma}^{-1} \tag{50}$$

so that:

$$\frac{\partial \boldsymbol{\Pi}_{\boldsymbol{\theta}}}{\partial \theta_i}\boldsymbol{u}=\frac{\partial \boldsymbol{u}}{\partial \theta_i} \tag{51}$$

Now, differentiating the projector to the second order yields:

$$\begin{aligned}\frac{\partial^2 \boldsymbol{\Pi}_{\boldsymbol{\theta}}}{\partial \theta_i \partial \theta_j}=&\frac{\partial^2 \boldsymbol{u}}{\partial \theta_i \partial \theta_j}\boldsymbol{u}^t\boldsymbol{\Sigma}^{-1}+\frac{\partial \boldsymbol{u}}{\partial \theta_i}\frac{\partial \boldsymbol{u}^t}{\partial \theta_j}\boldsymbol{\Sigma}^{-1}\\&+\frac{\partial \boldsymbol{u}}{\partial \theta_j}\frac{\partial \boldsymbol{u}^t}{\partial \theta_i}\boldsymbol{\Sigma}^{-1}+\boldsymbol{u}\frac{\partial^2 \boldsymbol{u}^t}{\partial \theta_i \partial \theta_j}\boldsymbol{\Sigma}^{-1}\end{aligned} \tag{52}$$

From (51), we deduce that:

$$\frac{\partial^2 \boldsymbol{\Pi}_{\boldsymbol{\theta}}}{\partial \theta_i \partial \theta_j}\boldsymbol{u}+\frac{\partial \boldsymbol{\Pi}_{\boldsymbol{\theta}}}{\partial \theta_i}\frac{\partial \boldsymbol{u}}{\partial \theta_j}=\frac{\partial^2 \boldsymbol{u}}{\partial \theta_i \partial \theta_j} \tag{53}$$

and then:

$$\begin{aligned}\boldsymbol{u}^t\boldsymbol{\Sigma}^{-1}\frac{\partial^2 \boldsymbol{\Pi}_{\boldsymbol{\theta}}}{\partial \theta_i \partial \theta_j}\boldsymbol{u}&=-\frac{\partial \boldsymbol{u}^t}{\partial \theta_i}\sum^{-1}\frac{\partial \boldsymbol{u}}{\partial \theta_j}-\boldsymbol{u}^t\boldsymbol{\Sigma}^{-1}\frac{\partial \boldsymbol{\Pi}_{\boldsymbol{\theta}}}{\partial \theta_i}\frac{\partial \boldsymbol{u}}{\partial \theta_j}\\&=-2\frac{\partial \boldsymbol{u}^t}{\partial \theta_i}\boldsymbol{\Sigma}^{-1}\frac{\partial \boldsymbol{u}}{\partial \theta_j}\end{aligned} \tag{54}$$

From (47) and (51), it can be inferred that:

$$\boldsymbol{s}^t\boldsymbol{\Sigma}^{-1}\frac{\partial \boldsymbol{\Pi}_{\boldsymbol{\theta}}}{\partial \theta_i}\boldsymbol{s}=K^2\boldsymbol{u}^t\boldsymbol{\Sigma}^{-1}\frac{\partial \boldsymbol{\Pi}_{\boldsymbol{\theta}}}{\partial \theta_i}\boldsymbol{u}=K^2\boldsymbol{u}^t\boldsymbol{\Sigma}^{-1}\frac{\partial \boldsymbol{u}}{\partial \theta_i}=0 \tag{55}$$

and from (54):

$$\begin{aligned}\boldsymbol{s}^t\boldsymbol{\Sigma}^{-1}\frac{\partial^2 \boldsymbol{\Pi}_{\boldsymbol{\theta}}}{\partial \theta_i \partial \theta_j}\boldsymbol{s}&=K^2\boldsymbol{u}^t\boldsymbol{\Sigma}^{-1}\frac{\partial^2 \boldsymbol{\Pi}_{\boldsymbol{\theta}}}{\partial \theta_i \partial \theta_j}\boldsymbol{u}\\&=-2K^2\frac{\partial \boldsymbol{u}^t}{\partial \theta_i}\boldsymbol{\Sigma}^{-1}\frac{\partial \boldsymbol{u}}{\partial \theta_j}\end{aligned} \tag{56}$$

Now, assuming that the SNR is not too weak, further approximations are realistic which consists in neglecting in (45) the third term and only keeping the first term in (46). Using (55) and (56), it leads to the following approximations:

$$\begin{aligned}[\boldsymbol{grad}(f)(\boldsymbol{\theta})]&\cong 2\left[\boldsymbol{s}^t\boldsymbol{\Sigma}^{-1}\frac{\partial \boldsymbol{\Pi}_{\boldsymbol{\theta}}}{\partial \theta_i}\boldsymbol{b}\right]_{i=1,\ldots,p}\\&=2\left[K\boldsymbol{u}^t\boldsymbol{\Sigma}^{-1}\frac{\partial \boldsymbol{\Pi}_{\boldsymbol{\theta}}}{\partial \theta_i}\boldsymbol{b}\right]_{i=1,\ldots,p}\\&=2\left[K\frac{\partial \boldsymbol{u}^t}{\partial \theta_i}\boldsymbol{\Sigma}^{-1}\boldsymbol{b}\right]_{i=1,\ldots,p}\end{aligned} \tag{57}$$

and:

$$\begin{aligned}[\boldsymbol{hess}(f)(\boldsymbol{\theta})]&\cong\left[\boldsymbol{s}^t\boldsymbol{\Sigma}^{-1}\frac{\partial^2 \boldsymbol{\Pi}_{\boldsymbol{\theta}}}{\partial \theta_i \partial \theta_j}\boldsymbol{s}\right]_{\substack{i=1,\ldots,p\\j=1,\ldots,p}}\\&=-2\left[K^2\frac{\partial \boldsymbol{u}^t}{\partial \theta_i}\boldsymbol{\Sigma}^{-1}\frac{\partial \boldsymbol{u}}{\partial \theta_j}\right]_{\substack{i=1,\ldots,p\\j=1,\ldots,p}}\end{aligned} \tag{58}$$

The hessian matrix has then the behaviour of a deterministic matrix and the maximum of the energies of projection can be simply viewed as a sum of two random variables. It just remains to derive their probability density function. For the first one, $f(\boldsymbol{\theta}_v)=|\boldsymbol{\Pi}_{\boldsymbol{\theta}}(\boldsymbol{s}+\boldsymbol{b})|^2$, it is straightforward to show that:

$$\begin{aligned}f(\boldsymbol{\theta})&=\langle \boldsymbol{z},\boldsymbol{u}(\boldsymbol{\theta})\rangle^2=\langle \boldsymbol{s}+\boldsymbol{b},\boldsymbol{u}(\boldsymbol{\theta})\rangle^2\\&=(K+\langle \boldsymbol{b},\boldsymbol{u}(\boldsymbol{\theta})\rangle)^2\rightarrow\chi_1^2(K^2)\end{aligned} \tag{59}$$

For the second random variable, we just have to note that:

$$\begin{aligned}&[\boldsymbol{grad}(f)(\boldsymbol{\theta})]\\&\cong\begin{bmatrix}2K\dfrac{\partial \boldsymbol{u}^t}{\partial \theta_1}\boldsymbol{\Sigma}^{-1}\boldsymbol{b}\\\vdots\\2K\dfrac{\partial \boldsymbol{u}^t}{\partial \theta_p}\boldsymbol{\Sigma}^{-1}\boldsymbol{b}\end{bmatrix}\\&\rightarrow N\left(\begin{bmatrix}0\\\vdots\\0\end{bmatrix},\left[4K^2\frac{\partial \boldsymbol{u}^t}{\partial \theta_i}\boldsymbol{\Sigma}^{-1}\frac{\partial \boldsymbol{u}}{\partial \theta_j}\right]_{\substack{i=1,\ldots,p\\j=1,\ldots,p}}\right)\end{aligned} \tag{60}$$

and then, it clearly appears that:

$$-\frac{1}{2}[\boldsymbol{grad}(f)(\boldsymbol{\theta})]^t[\boldsymbol{hess}(f)(\boldsymbol{\theta})]^{-1}[\boldsymbol{grad}(f)(\boldsymbol{\theta})]\rightarrow\chi_p^2 \tag{61}$$

with $p=3$. Now, we only have to prove the independence of the two random variables.

First, $f(\boldsymbol{\theta})$ is the square of a gaussian random variable equal to:

$$\langle \boldsymbol{z},\boldsymbol{u}\rangle=K+\boldsymbol{u}^t\boldsymbol{\Sigma}^{-1}\boldsymbol{b} \tag{62}$$

and the gradient is a gaussian random vector equal to:

$$[\boldsymbol{grad}(f)(\boldsymbol{\theta})]=\left[2K\frac{\partial \boldsymbol{u}^t}{\partial \theta_i}\boldsymbol{\Sigma}^{-1}\boldsymbol{b}\right]_{i=1,\ldots,p} \tag{63}$$

So, the calculation of the correlation between $f(\boldsymbol{\theta})$ and each component of the gradient vector gives:

$$\begin{aligned}&\boldsymbol{E}\left[\left(K+\boldsymbol{u}^t\boldsymbol{\Sigma}^{-1}\boldsymbol{b}\right)\left(2K\frac{\partial \boldsymbol{u}^t}{\partial \theta_i}\boldsymbol{\Sigma}^{-1}\boldsymbol{b}\right)\right]\\&=\boldsymbol{E}\left[\left(K+\boldsymbol{u}^t\boldsymbol{\Sigma}^{-1}\boldsymbol{b}\right)\left(2K\boldsymbol{b}^t\boldsymbol{\Sigma}^{-1}\frac{\partial \boldsymbol{u}}{\partial \theta_i}\right)\right]\\&=2K^2\boldsymbol{E}[\boldsymbol{b}^t]\boldsymbol{\Sigma}^{-1}\frac{\partial \boldsymbol{u}}{\partial \theta_i}\\&\quad+2K\boldsymbol{u}^t\boldsymbol{\Sigma}^{-1}\boldsymbol{E}[\boldsymbol{b}\boldsymbol{b}^t]\boldsymbol{\Sigma}^{-1}\frac{\partial \boldsymbol{u}}{\partial \theta_i}\\&=0+2K\boldsymbol{u}^t\boldsymbol{\Sigma}^{-1}\frac{\partial \boldsymbol{u}}{\partial \theta_i}=0\end{aligned} \tag{64}$$

So $\langle \boldsymbol{z},\boldsymbol{u}\rangle$ and each component of $[\boldsymbol{grad}(f)(\boldsymbol{\theta})]$ are uncorrelated. As they are also normal, they are independent.

The conclusion is that the probability density function of the maximum of the projection energies is a non-central khi-2 with $1+p=4$ degrees of freedom:

$$\sup_{\hat{\boldsymbol{o}}}f(\hat{\boldsymbol{\theta}})=\sup_{\hat{\boldsymbol{o}}}\left|{}_{\hat{\boldsymbol{\theta}}}\boldsymbol{z}\right|^2=2\log(\Lambda(\boldsymbol{z})_{\boldsymbol{\theta}=\hat{\boldsymbol{\theta}}})\rightarrow\chi_4^2(K^2) \tag{65}$$

This result is the same as the one given by Kendall and Stuart [17] and also Kay [18] but its validity is no longer limited to the case of independent identically distributed samples and we have established that this assumption is not required as long as the SNR remains strong enough.